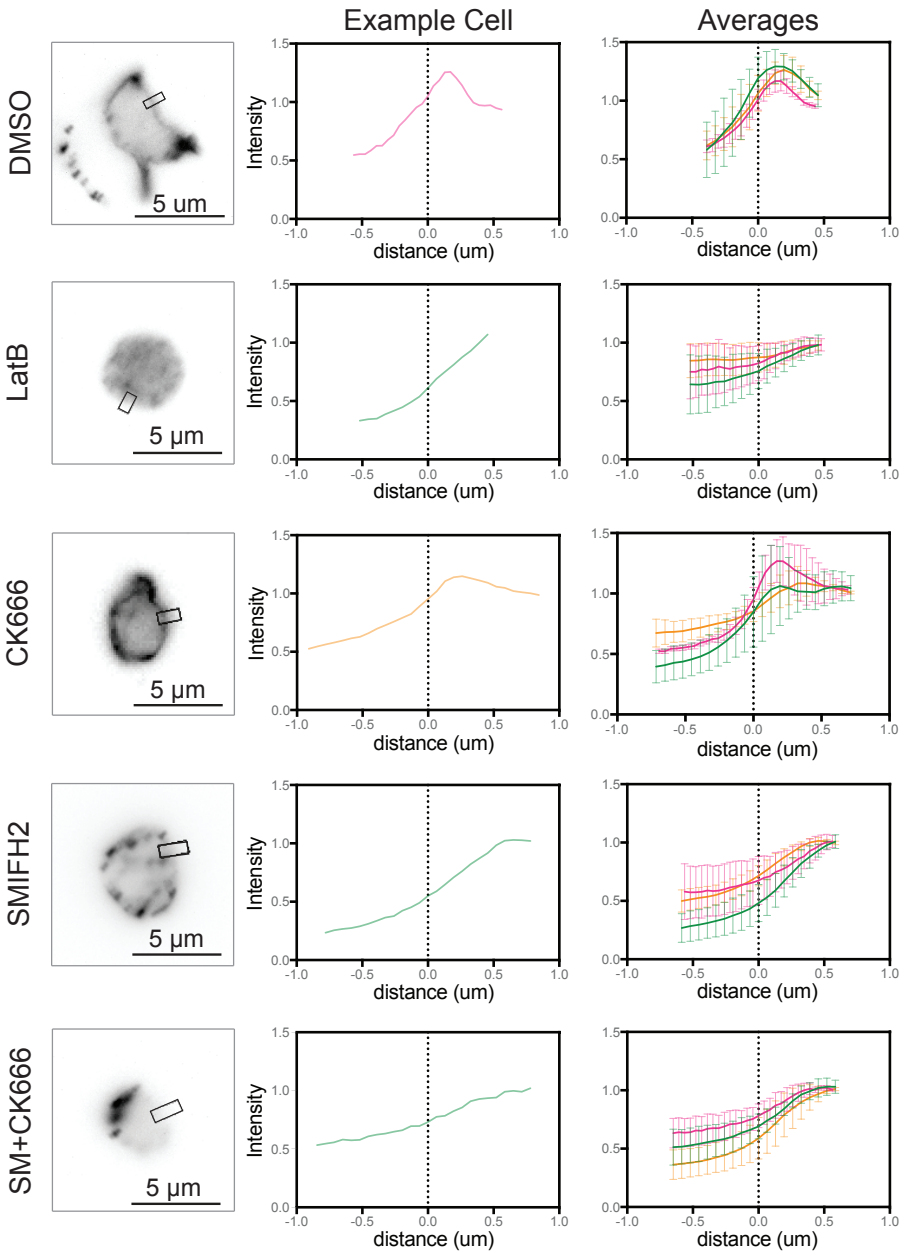

Figure S1. The actin cortex of *Bd* zoospores is dynamic and is affected by SMIFH2, related to Figure 1. Synchronized populations of *Bd* zoospores were treated with various actin inhibitors for 30 minutes (See **Figure 6** for concentrations). Cells were then fixed and stained for polymerized actin with fluorescent phalloidin, imaged, and line scans perpendicular to the cell edge were taken. Actin structures (inverted, black) in representative cells with the location of the line scan overlayed (left). Phalloidin intensity normalized to the cell interior plotted against distance along the line normalized with the cell edge at 0 µm for the cell shown (middle). Average intensities and standard deviations for three independent experiments (N=6 cells), normalized in the same way (right). Scale bars, 5 µm.

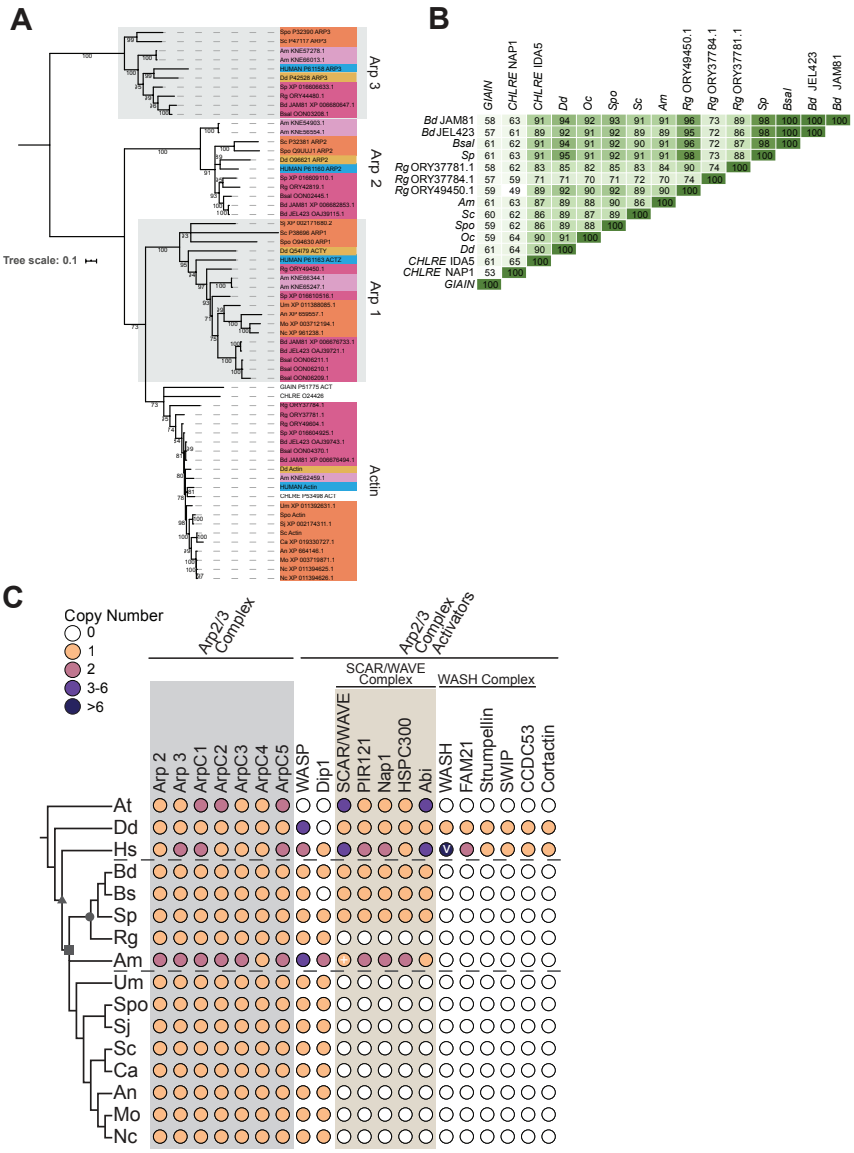

Figure S2. Chytrids have canonical actin as well as the Arp2/3 complex and many of its regulators, related to Figure 2. All chytrid sequences sharing ≥50% similarity with Rabbit, *Dictyostelium discoideum*, *Saccharomyces cerevisiae*, or *Schizosaccharomyces pombe* actin sequences were obtained using BLAST and aligned with known actin, Arp1, Arp2, and Arp3 sequences from various taxa. (Note: although rabbit and human muscle actin have identical protein sequences, we chose rabbit actin as the vast majority of biochemical characterization of animal actin has been done on rabbit actin.) (A) Percent similarities between the actin sequences of the given species. (B) Maximum likelihood phylogeny built to determine which chytrid sequences were true actin sequences. Consensus tree shown, branches with less than 70% bootstrap value were collapsed to polytomies. All bootstrap values shown. True chytrid actin sequences were determined as those that grouped with known actin sequences from other organisms. (C) The distribution of the Arp2/3 complex and its regulators across taxa. Color-filled circles indicate the presence of clear homologs found, with the number of homologs for each protein in each species shown in the colors specified in the key, whereas white dots indicate that no homolog was detected in that species. Dashed lines mark the chytrids. Symbols on the tree represent: opisthokonts (triangle); fungi (square); chytridiomycota (circle). V, copy number of WASH varies individually, as many WASH genes are subtelomeric [S1]. +, See **Data S2** for de-

tails and additional potential homologs with caveates. *At, Arabidopsis thaliana;* Rabbit/*Oc*, *Oryctolagus cuniculus*, HUMAN, *Homo sapiens, Dd, Dictyostelium discoideum; Bd, Batrachochytrium dendrobatidis (*JAM81 and JEL423 strains*); Bs, Batrachochytrium salamandrivorans; Sp, Spizellomyces punctatus; Rg, Rhizoclosmatium globosum; Am, Allomyces macrogynus; Sc, Saccharomyces cerevisiae; Spo, Schizosaccharomyces pombe; Sj, Schizosaccharomyces japonicus*; Ca, *Candida albicans*; An, *Aspergillus nidulans*; Mo, *Magnaporthe oryzae*; Nc, *Neurospora crassa*; Um, *Ustilago maydis; CHLRE, Chlamydomonas reinhardtii; GIAIN, Giardia intestinalis.*

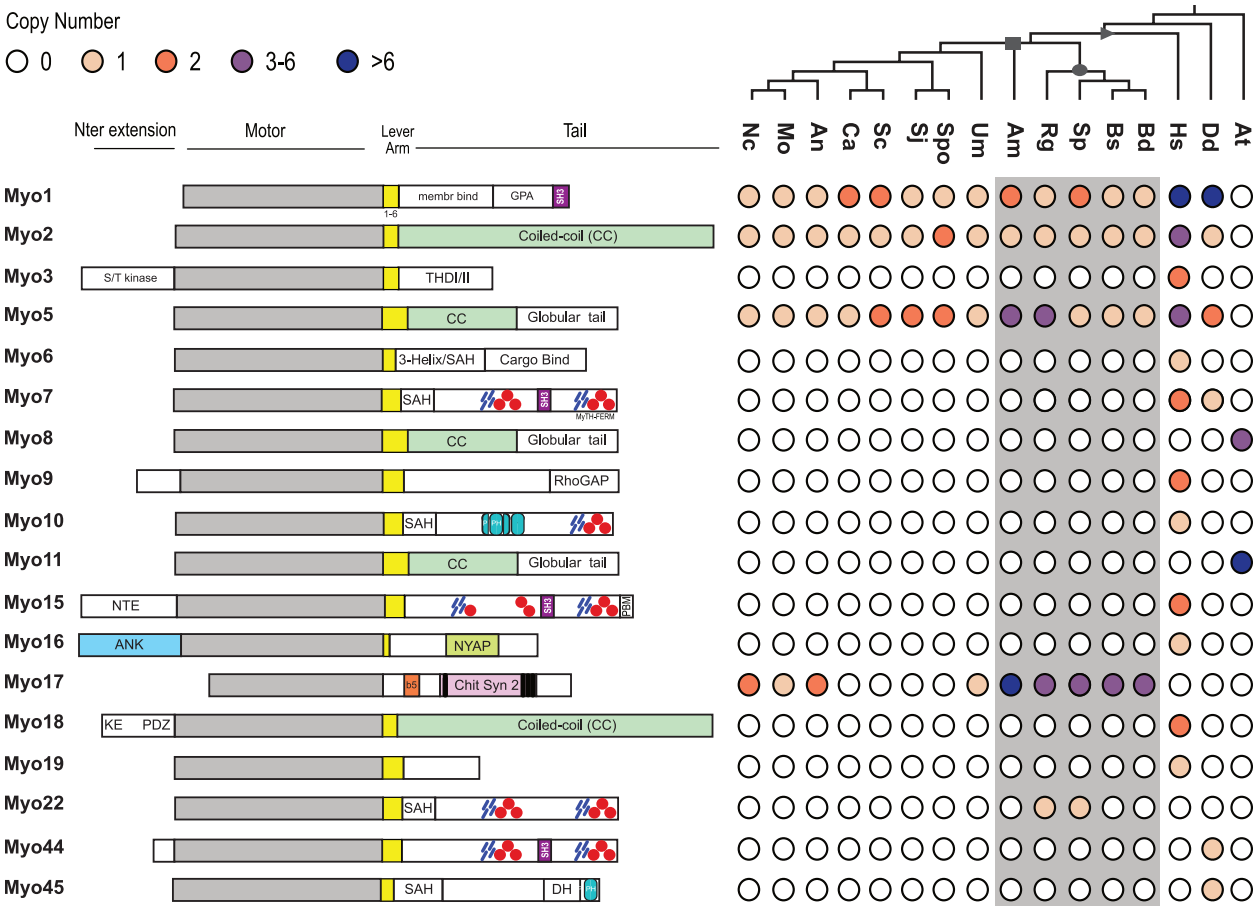

Figure S3. Chytrids have myosins from at least 4 classes, related to Figure 2. The distribution of given myosins (left, not to scale), across taxa (right). Color-filled circles indicate the presence of at least one myosin of that class in that species, with color indicating the number of myosins. Unfilled circles indicate that no myosin of that class was found in the given species. The domain abbreviations are as follows: yellow box, light chain binding domains (IQ motifs) that can vary in number; blue rectangles, MyTH4 domain; red circles, FERM domain; light blue oval, PH domain; black bars, transmembrane domain; membr binding, membrane binding; GPA, glycine-proline-alanine rich; SH3, src homology 3 (purple rectangle); S/T kinase, serine-threonine kinase; THDI/II, tail homology domain I/II; 3-Helix, triple helix bundle; SAH, single alpha-helix; NTE, N-terminal extension; PBM, PDZ binding motif; ANK, ankyrin repeats; NYAP, Neuronal tYrosine-phosphorylated Adaptor for the PI 3-kinase domain; b5, cytochrome heme binding domain; Chit syn 2, chitin synthase 2; KE, lysine and glutamate rich; PDZ, PDZ domain; DH, Dbl homology domain. *At, Arabidopsis thaliana; Dd, Dictyostelium discoideum; Hs, Homo sapiens* (non-muscle myosins only depicted)*; Bd, Batrachochytrium dendrobatidis; Bs, Batrachochytrium salamandrivorans; Sp, Spizellomyces punctatus; Rg, Rhizoclosmatium globosum; Am, Allomyces macrogynus; Sc, Saccharomyces cerevisiae; Spo, Schizosaccharomyces pombe; Sj, Schizosaccharomyces japonicus*; Ca, *Candida albicans*; An, *Aspergillus nidulans*; Mo, *Magnaporthe oryzae*; Nc, *Neurospora crassa*; Um, *Ustilago maydis.*

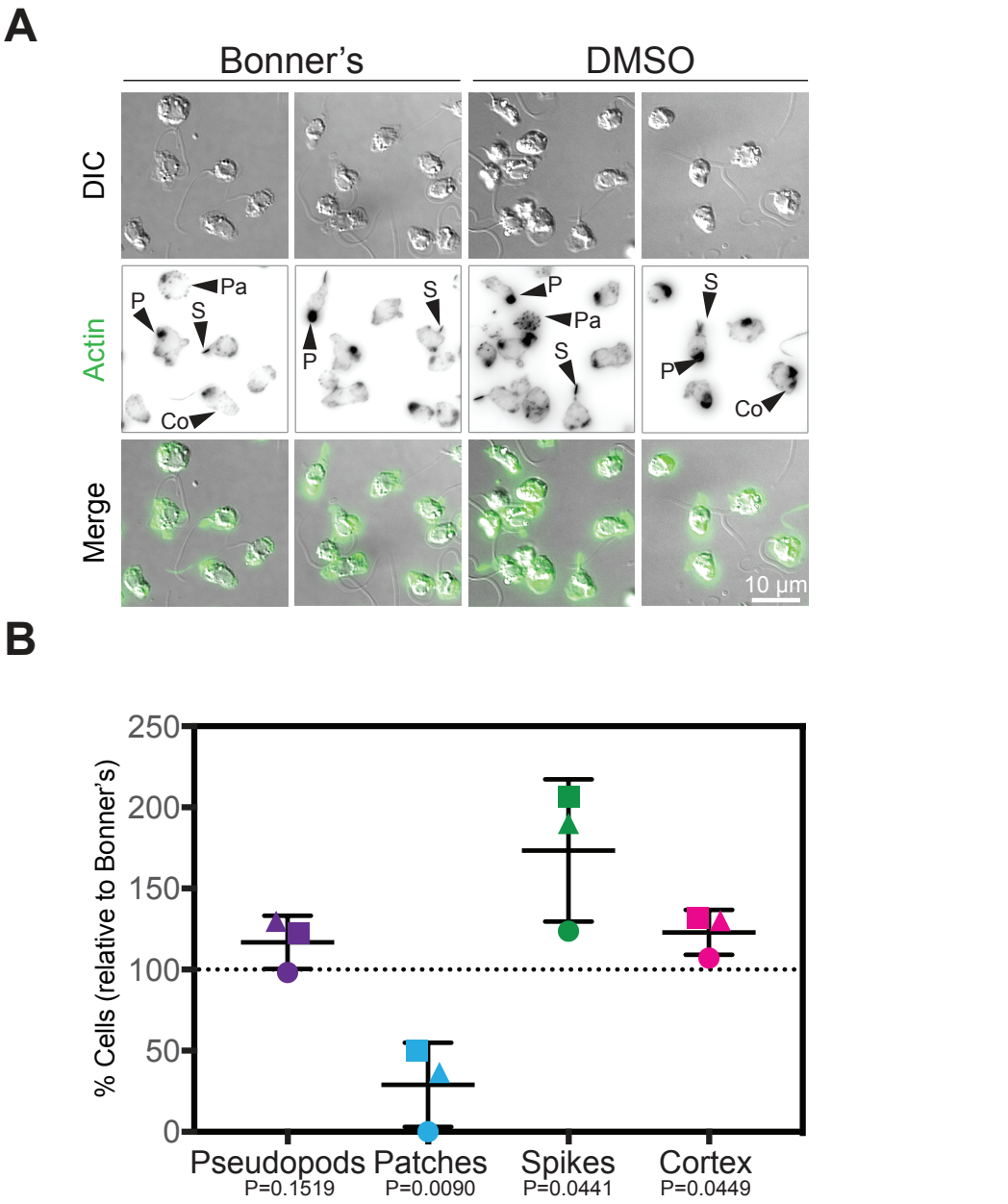

Figure S4. DMSO has an effect on the actin structures in *Bd,* related to Figure 6. Synchronized populations of *Bd* zoospores were treated with DMSO at the same concentration used in **Figure 6**, or equal volume of Bonner's salts as a control. Cells were then fixed and stained for polymerized actin with fluorescent phalloidin, imaged, and quantified for presence of actin-filled pseudopods (P, Pods), actin spikes (S), cortical actin (Co), and actin patches (P). (A) Representative examples of cells (DIC, grey) , and phalloidin stained actin structures (inverted, black), with an overlay of the two (actin, green) after treatment with Bonner's salts or DMSO. (B) Quantification of the percent of cells with each structure in the DMSO treated cells, normalized to the Bonner's salts control. P-values for each structure, relative to the Bonner's control, are shown (unpaired Student's T-tests). All fluorescent images are not at the same brightness and contrast scale. Scale bar, 10 µm.

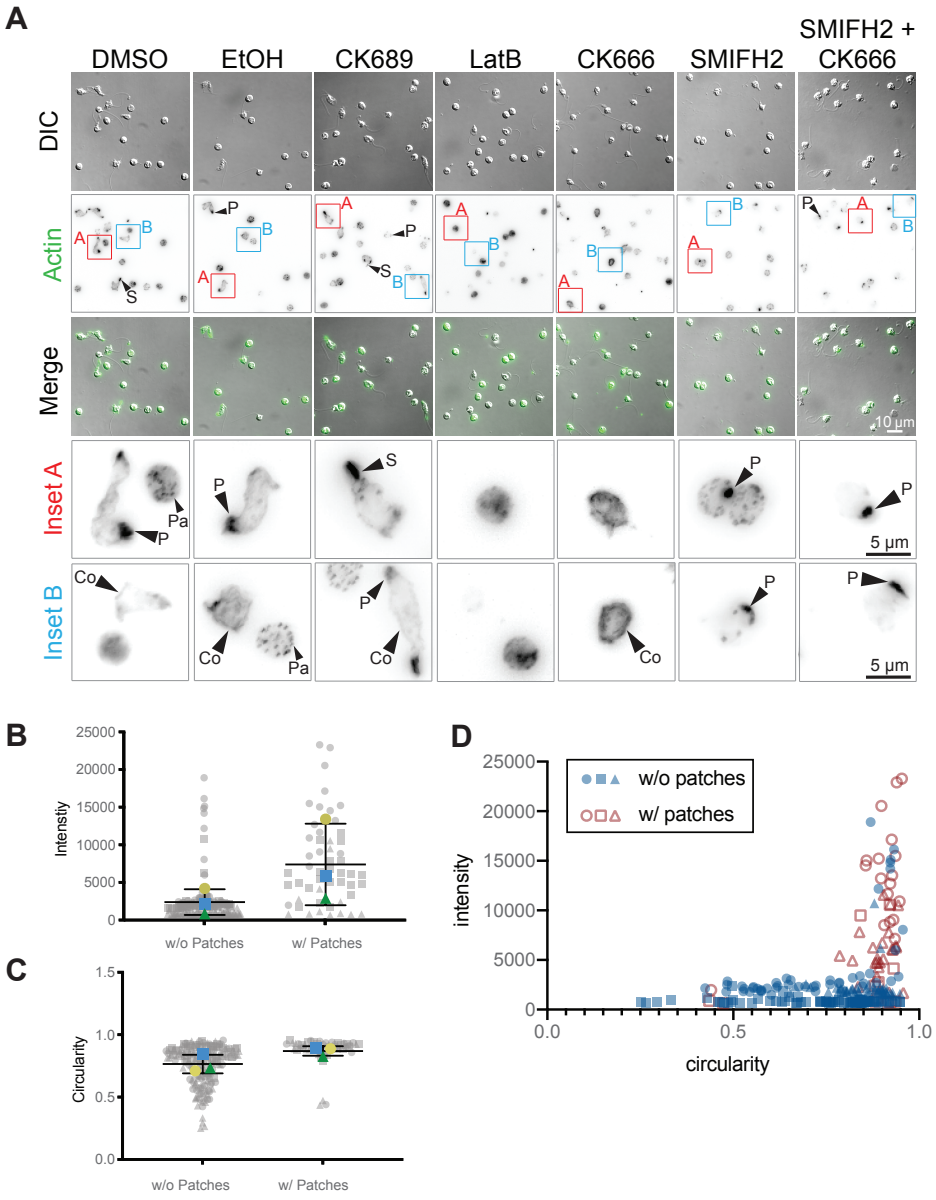

Figure S5. Additional examples of actin structures in *Bd* zoospores, related to Figure 6. Synchronized populations of *Bd* zoospores were treated with various actin inhibitors for 30 minutes (see **Figure 6** legend for concentrations). Cells were then fixed and stained for polymerized actin with fluorescent phalloidin and imaged. (A) Representative examples of zoospores (DIC: grey) and phalloidin stained actin structures (inverted, black) with an overlay of the two (actin, green) after treatment with each drug. Insets show an enlarged view of the actin channel for the indicated cells. Examples of pseudopods and spikes are highlighted, note pseudopods in SMIFH2 treated cells (highlighted by an arrowhead labeled P) are rounder and less protrusive. Pseudopods (P), actin spikes (S), cortical actin (Co), actin patches (Pa). Scale bar, 10 µm for field of view, 5 µm for insets. (B) Calcofluour white intensity for control cells without (w/o) and with (w/) actin patches. (C) Circularity values for control cells without and with actin patches. For B and C, Larger, colored circles indicate the average value for three independent replicates, represented by different shapes. Each gray shape represents the value of one cell in the indicated replicate. (D) Calcofluor white intensity plotted against circularity for control cells without (solid blue shapes) and with (outlined red shapes) actin patches. Each point represents a single cell from three independent replicates given their own shape.

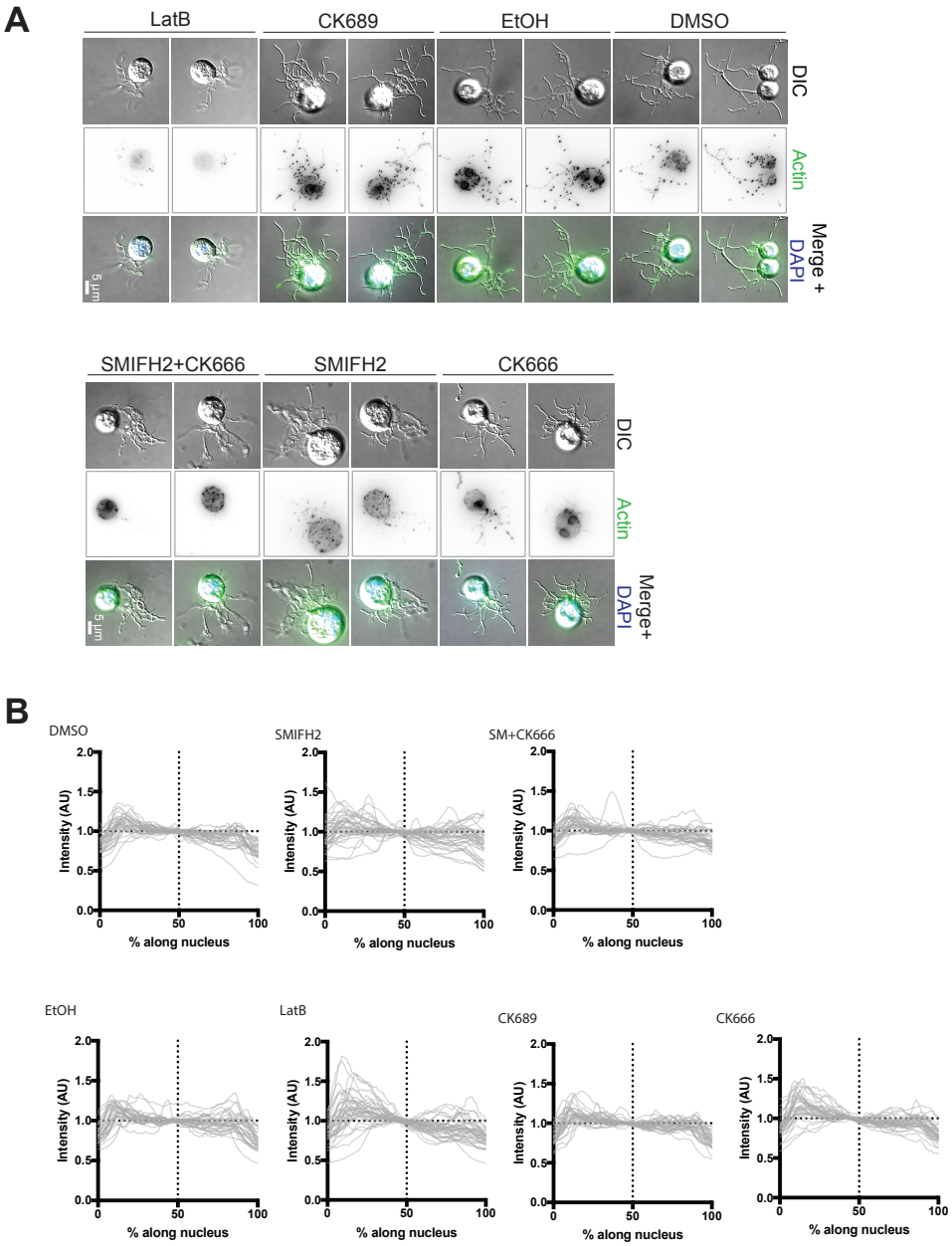

Figure S6. Additional examples of actin structures in *Bd* sporangia, related to Figure 7. Populations of *Bd* sporangia seeded 1 day prior were treated with drugs using the same concentrations as in Figure 6, then fixed and stained for polymerized actin with phalloidin and for DNA with DAPI. (A) Examples of sporangia (DIC: grey) and phalloidin stained actin patches (alone inverted, black; overlay, green), with an overlay including the nucleus (blue) after treatment with each drug. Scale bar, 5 µm. (B) Linescans of the intensity of actin in actin shells across nuclei in cells treated with the indicated actin inhibitors or controls. Actin intensity was normalized to the center of each line, and the distance of each line was normalized as a percent along the nucleus, as each line varied in size. The normalized intensity along each line is plotted such that the highest intensity is on the left.

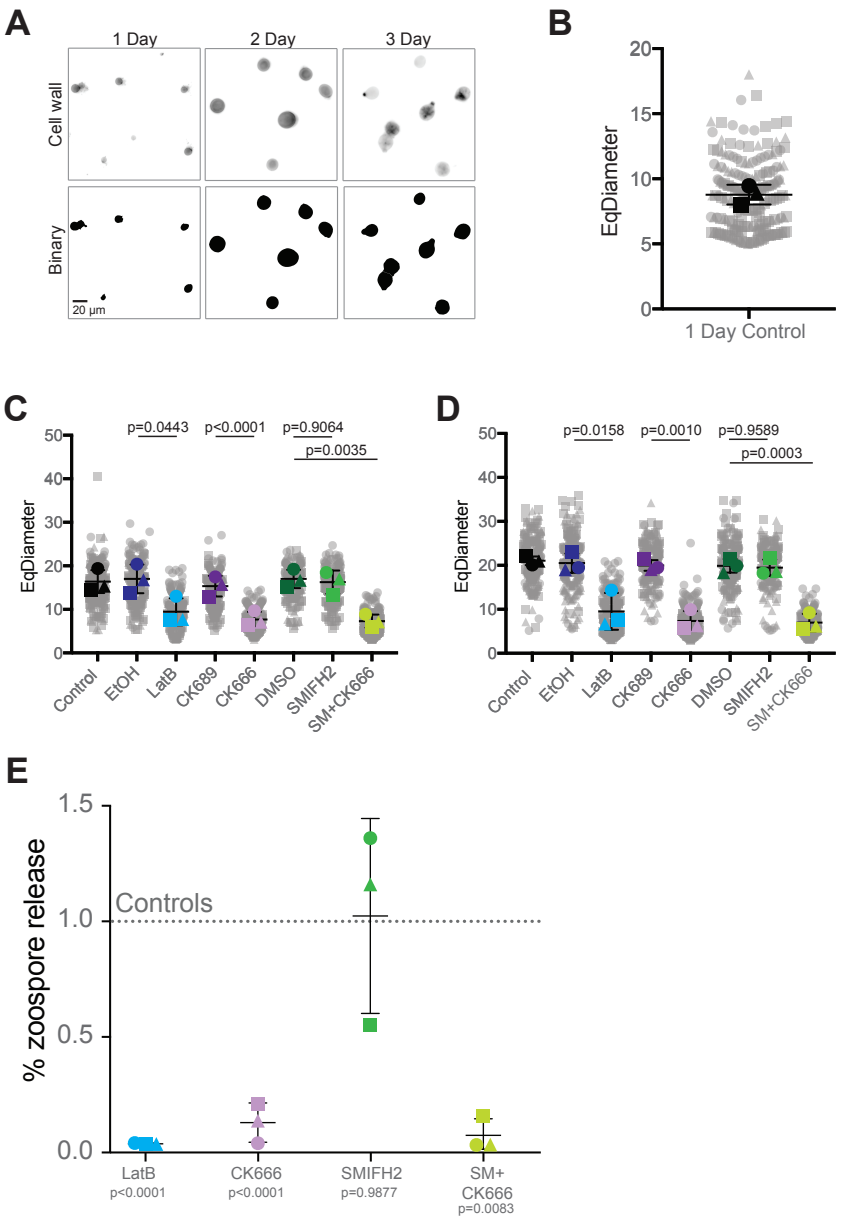

Figure S7. Long term inhibition of actin or Arp2/3 complex stunts growth and development of *Bd* sporangia, related to Figure 7. Populations of synchronized *Bd* zoospores were allowed to grow for 24 hours before the addition of actin inhibiting drugs at the same concentration as in Figure 6. Cells were treated for either 24 or 48 hours before being stained with Calcofluor White to highlight the cell wall and facilitate downstream image thresholding. The concentration of released zoospores was measured for cells treated for 48 hours prior to cell wall staining. (A) Examples of the thresholding binaries in control cells used for the analysis of sporangia size. The resulting binary objects were used to estimate the diameter of a sphere with the same area as the binary object (EqDiameter). (B) The EqDiameter for pre-treatment cells grown for 24 hours. (C) EqDiameter for cells that have grown for 24 hours prior to treatment, and for 24 hours with the indicated treatment. (D) EqDiameter for cells grown for 24 hours prior to treatment and for 48 hours with the indicated treatment. Large shapes indicate the average diameter of cells for three independent experiments. Each gray shape indicates the diameter for one cell in the given experiment. (E) The percent of zoospores released by 3-day sporangia after being treated with actin inhibiting drugs for 48 hours, normalized to appropriate controls. Scale bar, 20 5 µm.

Supplemental References

S1. Linardopoulou, E. V., Parghi, S. S., Friedman, C., Osborn, G. E., Parkhurst, S. M., and Trask, B. J. (2007). Human subtelomeric WASH genes encode a new subclass of the WASP family. PLoS Genet. *3*, e237.

S2. Carlsson, L., Nyström, L. E., Sundkvist, I., Markey, F., and Lindberg, U. (1977). Actin polymerizability is influenced by profilin, a low molecular weight protein in non-muscle cells. J. Mol. Biol. *115*, 465–483.

S3. Goldschmidt-Clermont, P. J., Furman, M. I., Wachsstock, D., Safer, D., Nachmias, V. T., and Pollard, T. D. (1992). The control of actin nucleotide exchange by thymosin beta 4 and profilin. A potential regulatory mechanism for actin polymerization in cells. Mol. Biol. Cell *3*, 1015–1024.

S4. Pruyne, D., Evangelista, M., Yang, C., Bi, E., Zigmond, S., Bretscher, A., and Boone, C. (2002). Role of formins in actin assembly: nucleation and barbed-end association. Science *297*, 612–615.

S5. Sagot, I., Rodal, A. A., Moseley, J., Goode, B. L., and Pellman, D. (2002). An actin nucleation mechanism mediated by Bni1 and profilin. Nat. Cell Biol. *4*, 626–631.

S6. Kovar, D. R., Kuhn, J. R., Tichy, A. L., and Pollard, T. D. (2003). The fission yeast cytokinesis formin Cdc12p is a barbed end actin filament capping protein gated by profilin. J. Cell Biol. *161*, 875–887.

S7. Zigmond, S. H., Evangelista, M., Boone, C., Yang, C., Dar, A. C., Sicheri, F., Forkey, J., and Pring, M. (2003). Formin leaky cap allows elongation in the presence of tight capping proteins. Curr. Biol. *13*, 1820–1823.

S8. Moseley, J. B., Sagot, I., Manning, A. L., Xu, Y., Eck, M. J., Pellman, D., and Goode, B. L. (2004). A conserved mechanism for Bni1- and mDia1-induced actin assembly and dual regulation of Bni1 by Bud6 and profilin. Mol. Biol. Cell *15*, 896–907.

S9. Romero, S., Le Clainche, C., Didry, D., Egile, C., Pantaloni, D., and Carlier, M.-F. (2004). Formin is a processive motor that requires profilin to accelerate actin assembly and associated ATP hydrolysis. Cell *119*, 419–429.

S10. Kovar, D. R., Harris, E. S., Mahaffy, R., Higgs, H. N., and Pollard, T. D. (2006). Control of the assembly of ATP- and ADP-actin by formins and profilin. Cell *124*, 423–435.

S11. Li, F., and Higgs, H. N. (2003). The mouse Formin mDia1 is a potent actin nucleation factor regulated by autoinhibition. Curr. Biol. *13*, 1335–1340.

S12. Quinlan, M. E., Heuser, J. E., Kerkhoff, E., and Mullins, R. D. (2005). Drosophila Spire is an actin nucleation factor. Nature *433*, 382–388.

S13. Ahuja, R., Pinyol, R., Reichenbach, N., Custer, L., Klingensmith, J., Kessels, M. M., and Qualmann, B. (2007). Cordon-bleu is an actin nucleation factor and controls neuronal morphology. Cell *131*, 337–350.

S14. Rebowski, G., Boczkowska, M., Hayes, D. B., Guo, L., Irving, T. C., and Dominguez, R. (2008). X-ray scattering study of actin polymerization nuclei assembled by tandem W domains. Proc Natl Acad Sci USA *105*, 10785–10790.

S15. Bradley, A. O., Vizcarra, C. L., Bailey, H. M., and Quinlan, M. E. (2020). Spire stimulates nucleation by Cappuccino and binds both ends of actin filaments. Mol. Biol. Cell *31*, 273–286.

S16. Ghoshdastider, U., Popp, D., Burtnick, L. D., and Robinson, R. C. (2013). The expanding superfamily of gelsolin homology domain proteins. Cytoskeleton (Hoboken) *70*, 775–795.

S17. Sebé-Pedrós, A., Roger, A. J., Lang, F. B., King, N., and Ruiz-Trillo, I. (2010). Ancient origin of the integrin-mediated adhesion and signaling machinery. Proc Natl Acad Sci USA *107*, 10142–10147.

S18. Bloemink, M. J., and Geeves, M. A. (2011). Shaking the myosin family tree: biochemical kinetics defines four types of myosin motor. Semin. Cell Dev. Biol. *22*, 961–967.

S19. Masters, T. A., Kendrick-Jones, J., and Buss, F. (2017). Myosins: domain organisation, motor properties, physiological roles and cellular functions. Handb. Exp. Pharmacol. *235*, 77–122.

S20. Odronitz, F., and Kollmar, M. (2007). Drawing the tree of eukaryotic life based on the analysis of 2,269 manually annotated myosins from 328 species. Genome Biol. *8*, R196.

S21. Kollmar, M., and Mühlhausen, S. (2017). Myosin repertoire expansion coincides with eukaryotic diversification in the Mesoproterozoic era. BMC Evol. Biol. *17*, 211.

S22. McIntosh, B. B., and Ostap, E. M. (2016). Myosin-I molecular motors at a glance. J. Cell Sci. *129*, 2689–2695.

S23. Giblin, J., Fernández-Golbano, I. M., Idrissi, F.-Z., and Geli, M. I. (2011). Function and regulation of Saccharomyces cerevisiae myosins-I in endocytic budding. Biochem. Soc. Trans. *39*, 1185–1190.

S24. Oberholzer, U., Marcil, A., Leberer, E., Thomas, D. Y., and Whiteway, M. (2002). Myosin I is required for hypha formation in Candida albicans. Eukaryotic Cell *1*, 213–228.

S25. Lara-Rojas, F., Bartnicki-García, S., and Mouriño-Pérez, R. R. (2016). Localization and role of MYO-1, an endocytic protein in hyphae of Neurospora crassa. Fungal Genet. Biol. *88*, 24–34.

S26. Medina, E. M., Robinson, K. A., Bellingham-Johnstun, K., Ianiri, G., Laplante, C., Fritz-Laylin, L. K., and Buchler, N. E. (2020). Genetic transformation of Spizellomyces punctatus, a resource for studying chytrid biology and evolutionary cell biology. elife *9*.

S27. West-Foyle, H., and Robinson, D. N. (2012). Cytokinesis mechanics and mechanosensing. Cytoskeleton (Hoboken) *69*, 700–709.

S28. Fritz-Laylin, L. K., Prochnik, S. E., Ginger, M. L., Dacks, J. B., Carpenter, M. L., Field, M. C., Kuo, A., Paredez, A., Chapman, J., Pham, J., et al. (2010). The genome of Naegleria gruberi illuminates early eukaryotic versatility. Cell *140*, 631–642.

S29. Aguilar-Cuenca, R., Juanes-García, A., and Vicente-Manzanares, M. (2014). Myosin II in mechanotransduction: master and commander of cell migration, morphogenesis, and cancer. Cell. Mol. Life Sci. *71*, 479–492.

S30. Rodriguez, J. R., and Paterson, B. M. (1990). Yeast myosin heavy chain mutant: maintenance of the cell type specific budding pattern and the normal deposition of chitin and cell wall components requires an intact myosin heavy chain gene. Cell Motil. Cytoskeleton *17*, 301–308.

S31. Titus, M. A. (2018). Myosin-Driven Intracellular Transport. Cold Spring Harb. Perspect. Biol. *10*.

S32. Hammer, J. A., and Sellers, J. R. (2011). Walking to work: roles for class V myosins as cargo transporters. Nat. Rev. Mol. Cell Biol. *13*, 13–26.

S33. Matsui, Y. (2003). Polarized distribution of intracellular components by class V myosins in Saccharomyces cerevisiae. Int. Rev. Cytol. *229*, 1–42.

S34. Weiss, I. M., Schönitzer, V., Eichner, N., and Sumper, M. (2006). The chitin synthase involved in marine bivalve mollusk shell formation contains a myosin domain. FEBS Lett. *580*, 1846–1852.

S35. Takeshita, N., Yamashita, S., Ohta, A., and Horiuchi, H. (2006). Aspergillus nidulans class V and VI chitin synthases CsmA and CsmB, each with a myosin motor-like domain, perform compensatory functions that are essential for hyphal tip growth. Mol. Microbiol. *59*, 1380–1394.

S36. Gandía, M., Harries, E., and Marcos, J. F. (2014). The myosin motor domain-containing chitin synthase PdChsVII is required for development, cell wall integrity and virulence in the citrus postharvest pathogen Penicillium digitatum. Fungal Genet. Biol. *67*, 58–70.

S37. Fajardo-Somera, R. A., Jöhnk, B., Bayram, Ö., Valerius, O., Braus, G. H., and Riquelme, M. (2015). Dissecting the function of the different chitin synthases in vegetative growth and sexual development in Neurospora crassa. Fungal Genet. Biol. *75*, 30–45.

S38. Schuster, M., Treitschke, S., Kilaru, S., Molloy, J., Harmer, N. J., and Steinberg, G. (2012). Myosin-5, kinesin-1 and myosin-17 cooperate in secretion of fungal chitin synthase. EMBO J. *31*, 214–227.

S39. Takeshita, N., Ohta, A., and Horiuchi, H. (2005). CsmA, a class V chitin synthase with a myosin motor-like domain, is localized through direct interaction with the actin cytoskeleton in Aspergillus nidulans. Mol. Biol. Cell *16*, 1961–1970.

S40. Treitschke, S., Doehlemann, G., Schuster, M., and Steinberg, G. (2010). The myosin motor domain of fungal chitin synthase V is dispensable for vesicle motility but required for virulence of the maize pathogen Ustilago maydis. Plant Cell *22*, 2476–2494.

S41. Tuxworth, R. I., Weber, I., Wessels, D., Addicks, G. C., Soll, D. R., Gerisch, G., and Titus, M. A. (2001). A role for myosin VII in dynamic cell adhesion. Curr. Biol. *11*, 318–329.

S42. Petersen, K. J., Goodson, H. V., Arthur, A. L., Luxton, G. W. G., Houdusse, A., and Titus, M. A. (2016). MyTH4-FERM myosins have an ancient and conserved role in filopod formation. Proc Natl Acad Sci USA *113*, E8059–E8068.

S43. Weck, M. L., Grega-Larson, N. E., and Tyska, M. J. (2017). MyTH4-FERM myosins in the assembly and maintenance of actin-based protrusions. Curr. Opin. Cell Biol. *44*, 68–78.

S44. Gibson, M. M., Bagga, D. A., Miller, C. G., and Maguire, M. E. (1991). Magnesium transport in Salmonella typhimurium: the influence of new mutations conferring Co2+ resistance on the CorA Mg2+ transport system. Mol. Microbiol. *5*, 2753–2762.

S45. Ilyin, G. P., Rialland, M., Pigeon, C., and Guguen-Guillouzo, C. (2000). cDNA cloning and expression analysis of new members of the mammalian F-box protein family. Genomics *67*, 40–47.

S46. Hegsted, A., Yingling, C. V., and Pruyne, D. (2017). Inverted formins: A subfamily of atypical formins. Cytoskeleton (Hoboken) *74*, 405–419.

S47. Moseley, J. B., and Goode, B. L. (2005). Differential activities and regulation of Saccharomyces cerevisiae formin proteins Bni1 and Bnr1 by Bud6. J. Biol. Chem. *280*, 28023–28033.

S48. Ruzicka, D. R., Kandasamy, M. K., McKinney, E. C., Burgos-Rivera, B., and Meagher, R. B. (2007). The ancient subclasses of Arabidopsis Actin Depolymerizing Factor genes exhibit novel and differential expression. Plant J. *52*, 460–472.

S49. Banuett, F., Quintanilla, R. H., and Reynaga-Peña, C. G. (2008). The machinery for cell polarity, cell morphogenesis, and the cytoskeleton in the Basidiomycete fungus Ustilago maydis-a survey of the genome sequence. Fungal Genet. Biol. *45 Suppl 1*, S3–S14.

S50. Higgs, H. N. (2005). Formin proteins: a domain-based approach. Trends Biochem. Sci. *30*, 342–353.

S51. El-Gebali, S., Mistry, J., Bateman, A., Eddy, S. R., Luciani, A., Potter, S. C., Qureshi, M., Richardson, L. J., Salazar, G. A., Smart, A., et al. (2019). The Pfam protein families database in 2019. Nucleic Acids Res. *47*, D427–D432.

S52. Trifinopoulos, J., Nguyen, L.-T., von Haeseler, A., and Minh, B. Q. (2016). W-IQ-TREE: a fast online phylogenetic tool for maximum likelihood analysis. Nucleic Acids Res. *44*, W232-5.